Available online at www.sciencedirect.com
ScienceDirect
Fluid Dynamics Research 38 (2006) 772–786
FLUID DYNAMICS RESEARCH

Two-phase flow in microchannels with surface modifications

Thomas Cubaud, Umberto Ulmanella, Chih-Ming Ho*

Mechanical and Aerospace Engineering Department, University of California, Los Angeles, 420 Westwood Plaza, Los Angeles, CA 90095-1597, USA

Received 24 July 2004; received in revised form 26 October 2005; accepted 27 December 2005

Communicated by Y. Matsumoto

Abstract

Two-phase flows in microchannels with surface modifications are experimentally investigated. First, we investigate the shape of static and moving bubbles in microchannels with square cross-sections for different contact angles. Water and air are mixed on-chip in a cross-shaped mixing chamber. This mixing geometry allows for the production of monodisperse bubbles, the size of which can be controlled with the flow rates. We study the flow morphologies of mixtures made of pure water and air, and made of water with surfactant and air (aqueous foam), in both hydrophilic and hydrophobic microchannels. Second, we investigate the transient rheological behavior of polymer solutions when the length of the polymers is comparable to the height of the channel. The measured viscosity of the solution is several times larger than the expected value, and does not show the typical shear-thinning behavior. These experiments highlight the importance of wall properties for two-phase flows in microfluidic devices.

PACS: 47.55.Kf; 81.65.−b; 83.10.Lk; 83.10.Nn

Keywords: Patterns; Multiphase flows; Polymers; Microfluidic; Nanofluidic; Surface treatment; Foam

1. Introduction

Multiphase flows are encountered in a wide range of industrial applications. They are prevalent in processes as diverse as oil recovery, food manufacturing, cosmetic production, nuclear power plant

* Corresponding author. Tel.: +1 310 825 9993; fax: +1 310 206 2302.
E-mail address: chihming@ucla.edu (C.-M. Ho).

0169-5983/$30.00
doi:10.1016/j.fluiddyn.2005.12.004

cooling, and fire-fighting. Miniaturization of fluidic devices has made it possible to precisely control bubble or droplet size (Thorsen et al., 2001; Link et al., 2004; Cubaud et al., 2005). Manipulating multiphase flows at the microscale allows for the development of portable power generation devices such as Micro Direct Methanol Fuel Cells (Yen et al., 2003).

As the dimension shrinks to micrometric scale, the relative importance of surface to volume forces increases. As a result, surface tension and viscous forces become predominant compared to inertia and buoyancy forces. Capillary forces are particularly sensitive to geometrical and interfacial properties. In microfluidic devices, modifications of interfacial properties between phases and solid surfaces greatly influence the multiphase flow morphologies. Surface treatment is usually achieved by flowing functional macromolecules through the device. For instance, reconfigurable hydrophobic–hydrophilic surfaces can be achieved by adsorption and removal of avidin from hydrophobic self-assembled monolayers (Deval et al., 2004). However, when the characteristic cross-sectional length of the channel becomes comparable to the size of the macromolecules, the rheological behaviors of the solution considerably depart from those observed in larger channels. This type of flow may be viewed as a two-phase flow of elastic solid particles in a liquid medium.

This paper is composed of two parts. First, we present a comprehensive but not exhaustive overview of liquid/gas flows in square cross-section microchannels with surface modifications. We investigate the shape of static and moving bubbles in square microchannels for different contact angles. Liquid and gas are mixed on-chip in a cross-shaped mixing chamber. This mixing process produces an array of monodisperse bubbles, the size of which is determined by the flow rates. We study the flow morphologies of mixtures made of pure water and air, and made of water with surfactant and air (aqueous foam), in both hydrophilic and hydrophobic microchannels. This study shows how specific liquid/gas flow morphologies can be produced at the micrometer scale with surface modifications. Second, we investigate the flow of polymer solutions in microgeometries. We experimentally measure the transient response of a polyacrylamide (PAAm) solution flowing in channels of 10 and 101.5 μm in diameter. Our results show that for the 10 μm channel, the measured viscosity is several times larger than in the 101.5 μm channel, and that the typical shear-thinning behavior is not observed. Moreover, the time scale associated with the transient flow in the 10 μm channel is on the order of 10 h compared to a few seconds for the 101.5 μm channel. This time scale could have important implications for practical use.

2. Liquid/gas flow in square microchannels

We investigate the effect of wettability on the flow morphologies of a mixture composed of pure water and air, as well as a mixture composed of water with surfactant and air. As surfactant is absorbed at the interfaces, it lowers the interfacial energies, stabilizes the flow against coalescence and leads to specific flow structures.

The shape of a static elongated bubble in a polygonal capillary composed of N sides depends on N and the contact angle θ (Concus and Finn, 1974). When $\theta < \pi/N$, liquid fills the channel wedges, and when $\theta > \pi/N$, gas fills the entire channel cross-section. Fig. 1 displays experimental pictures of a static elongated gas bubble in a square capillary ($N = 4$). The contact angle θ is the boundary condition that sets the shape of the liquid/gas interface. In the transition from partially non-wetting surfaces ($\theta > \pi/2$) to partially wetting surfaces ($\theta < \pi/2$), there is an inversion of the sign of the liquid/gas curvature (Figs. 1(a)

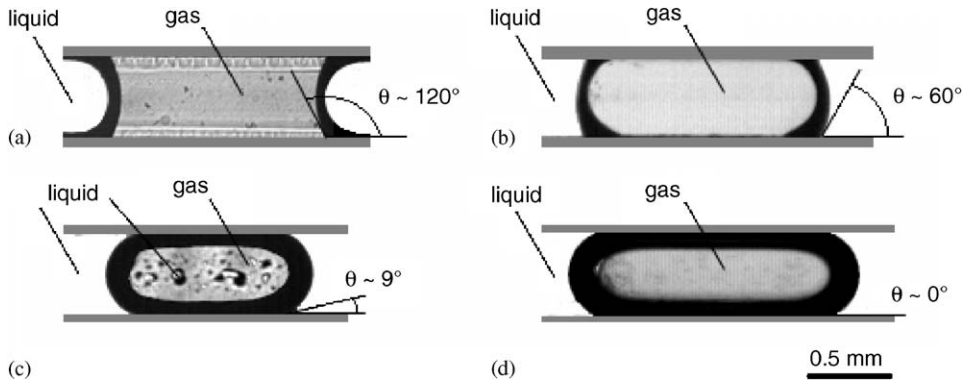

Fig. 1. Shapes of static bubble in square microchannel for different contact angles. (a) Hydrophobic plug bubble, (b) hydrophilic plug bubble, (c) wedging bubble with contact line, (d) lubricated bubble. The dark color represents a large liquid/gas curvature.

and (b)). When $0 < \theta < \pi/4$, the bubble does not fill the wedges of the channel (Fig. 1(c)). The system lowers its energy by creating a triple line (liquid/solid/gas) and gas directly contacts the center of the channel walls where small liquid droplets may be present. For a completely wetted system ($\theta = 0$), the gas bubble is lubricated by a liquid film (Fig. 1(d)).

When motion is induced, contact angle hysteresis increases the complexity of the system. The contact angle is defined with respect to the liquid; the advancing contact angle is at the rear of the bubble and the receding contact angle is at the front of the bubble. As velocity increases, the advancing contact angle increases and the receding contact angle decreases. Thus, the bubble shape loses symmetry with respect to the direction of the flow. Since contact angles are influenced by roughness and heterogeneities of the solid surface (Cubaud and Fermigier, 2004), moving bubbles may lose their symmetry with respect to the center axis of the channel. We experimentally investigate flow patterns when liquid and gas are flowing into square cross-sectional microchannels.

2.1. Experimental setup

Fig. 2 presents the schematics of the devices used to study liquid/gas flow in microchannels. Channels are made with glass and silicon using microfabrication techniques. Silicon is selectively etched to different depths using Deep Reactive Ion Etching. Pyrex glass pieces are anodically bonded to the top and bottom of the silicon to provide optical access to the flow. Static contact angles are measured for pure water and air on silicon ($\theta_{\text{sil}} \approx 9°$) and glass ($\theta_{\text{glass}} \approx 25°$). Fluids are supplied to the device with flexible tubes from pressurized reservoirs that have miniature regulators to adjust pressure. Flow rates are measured at the channel entrances. A high-speed camera (Redlake, Motionpro, 10,000 fps) is used with a fiber light to analyze the flow patterns. The camera is either mounted on a microscope or on a 60 mm lens with an extension tube.

The channel module is composed of two parts: a small mixing section (50 μm square channels), used to produce the homogeneous liquid/gas flows; and a test section (525 μm square channels), where the flow is investigated.

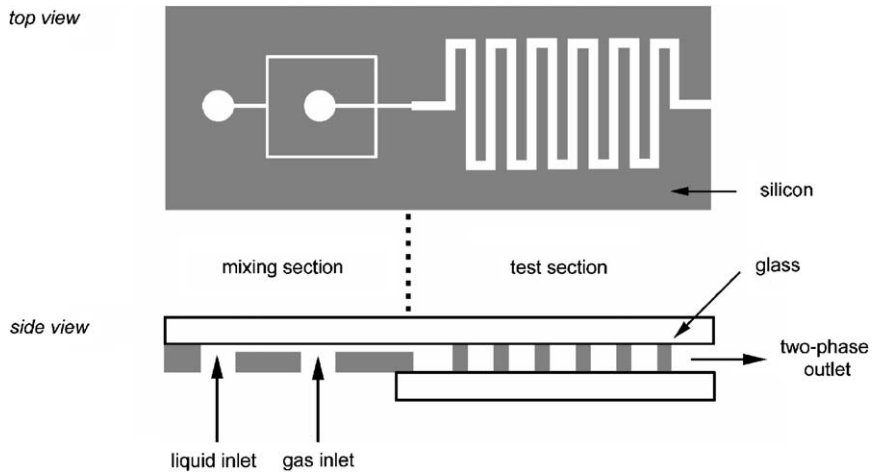

Fig. 2. Liquid/gas flow microchannel module.

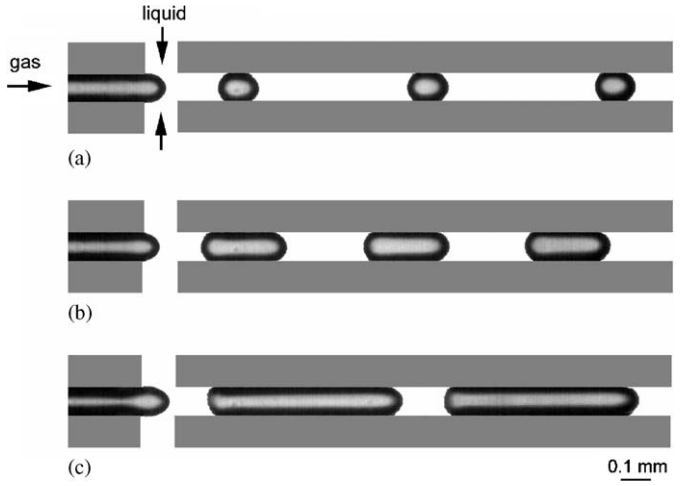

Fig. 3. On-chip mixing section. (a) $\alpha_G \approx 0.22$, (b) 0.53, (c) 0.82.

2.2. Mixing section

The method of producing two-phase flows determines the flow patterns. Fig. 3 shows the small liquid/gas mixing section where bubbles are produced with liquid cross flow. Liquid is introduced from the two sides of the central gas channel in order to pinch the gas flow and form bubbles. Well-defined bubbles in a wide range of sizes can be produced as a function of liquid and gas flow rates (Cubaud et al., 2005). The relative proportion of liquid and gas in the channel can be characterized with the homogeneous void fraction $\alpha_G = Q_G/(Q_G + Q_L)$, where Q_G and Q_L are, respectively, the gas and liquid flow rates. As can be seen in Fig. 3, as α_G increases, the size of the bubbles produced increases.

2.3. Pure water/air flow patterns

Two-phase flows are distributed into flow patterns depending on the liquid and gas flow rates, and on fluid and channel properties.

2.3.1. Hydrophilic flows

Between low and high void fractions, five main flow regimes are observed in partially wetting square microchannels: bubbly, wedging, slug, annular and dry flows. These can be seen in Fig. 4.

(a) The bubbly flow is composed of discrete spherical gas bubbles distributed in the liquid. The length d of the bubble is smaller than the channel width h. As bubbles collide and coalesce to form larger bubbles, polydispersity is observed. This motion is influenced by gravity.

(b) The wedging flow is made of elongated bubbles. Bubbles are equally spaced and relatively monodisperse. Depending on the bubble size and velocity, gas may dry out the center of the channel creating contact lines. Dry patches grow from the film instability. Liquid droplets may be present on the walls inside moving gas bubbles.

(c) The slug flow consists of long elongated bubbles lubricated by a liquid film between the gas and the walls. The nose of bubbles has a characteristic bullet-shape. Kolb and Cerro (1993) studied the transition from a non-axisymmetric to an axisymmetric bubble nose profile as a function of the capillary number, $Ca = \eta U/\gamma$, where η is the liquid viscosity, U is the bubble front velocity, and γ is the surface tension. The difference between the wedging and the slug flow is essentially due to the thickness of the liquid film between the bubbles and the center of the walls. For the wedging flow, the film is metastable and can break by nucleation of dewetting patches. For the slug flow, the film is stable and its thickness increases with the capillary number (Cubaud and Ho, 2004).

(d) The flow becomes annular when the bubble length is equal to the channel length. Gas continually flows in the center of the channel, while liquid experiences wall shear. Unstable liquid rings grow and vanish around the central bubble due to the large slip between the two phases.

(e) When the void fraction is close to unity, liquid is confined to flow in the channel wedges. The gas dries the center of the channel wall. The volume of liquid in the wedges decreases until the flow becomes a single gas phase.

Characterizing liquid/gas flows in hydrophilic channels is of prime importance in understanding the energy requirements for flowing bubbles in microfluidic devices such as Micro Direct Methanol Fuel Cells (Yen et al., 2003). In a previous investigation (Cubaud and Ho, 2004), we reported the dependency of the pressure drop on the flow characteristics.

2.3.2. Hydrophobic flows

Channels were coated with Teflon producing a static contact angle $\theta \approx 120^\circ$ for pure water and air. Liquid/gas flows in hydrophobic channels are very different from the ones observed in hydrophilic channels. In hydrophobic channels, bubbles are not lubricated and their motion is subject to contact line friction at the channel walls. Contact angle hysteresis can be seen in Figs. 5(a) and (b). In these figures, the advancing contact angle $\theta_{adv} > \pi/2$, the receding contact angle $\theta_{rec} < \pi/2$, and the interface curvature follows the flow direction. Small bubbles are trapped in the sharp channel corners. Although the hydrophobic flow is quite unsteady, three distinct flow patterns are identified for different void fractions as shown in Fig. 5.

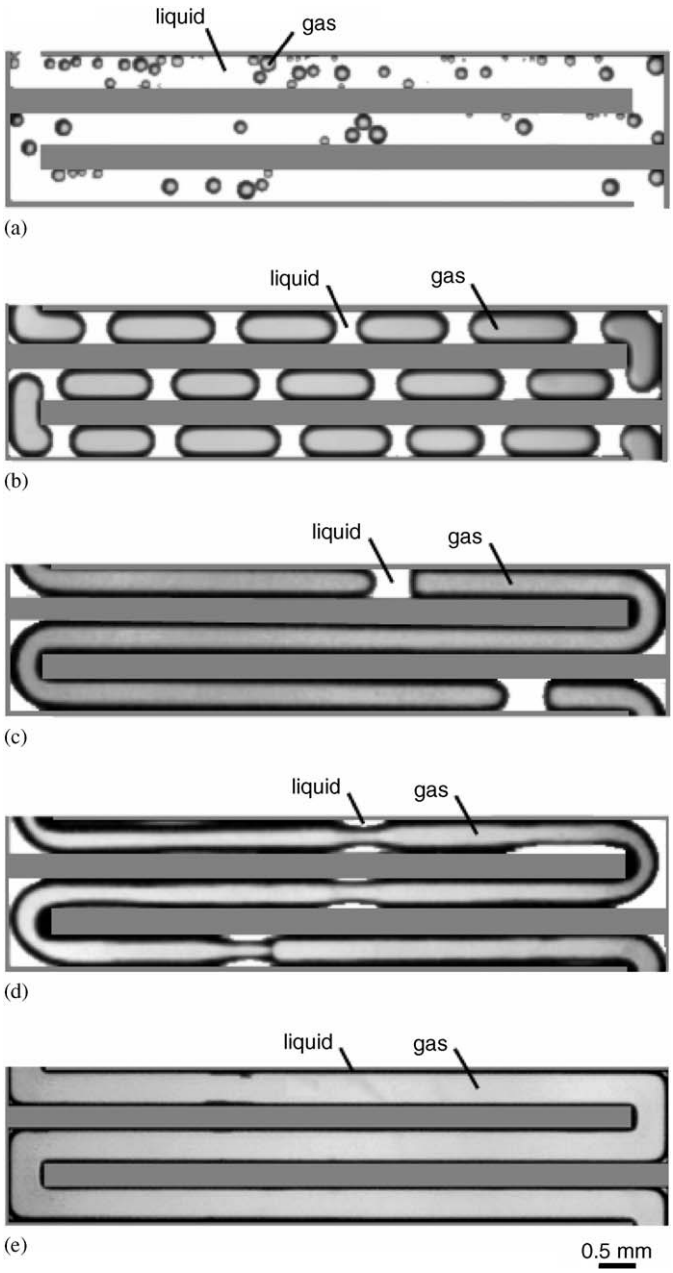

Fig. 4. Pure water/air flow patterns in hydrophilic channels. From low to high void fractions. (a) Bubbly flow, (b) wedging flow, (c) slug flow, (d) annular flow, (e) dry flow.

(a) Isolated asymmetric bubble flow is observed in the case of low void fractions, since the surface energy is low, small bubbles adhere to the channel walls. After many bubbles merge together, a large gas plug occupying the entire channel cross-section is formed and is pushed by the liquid flow.

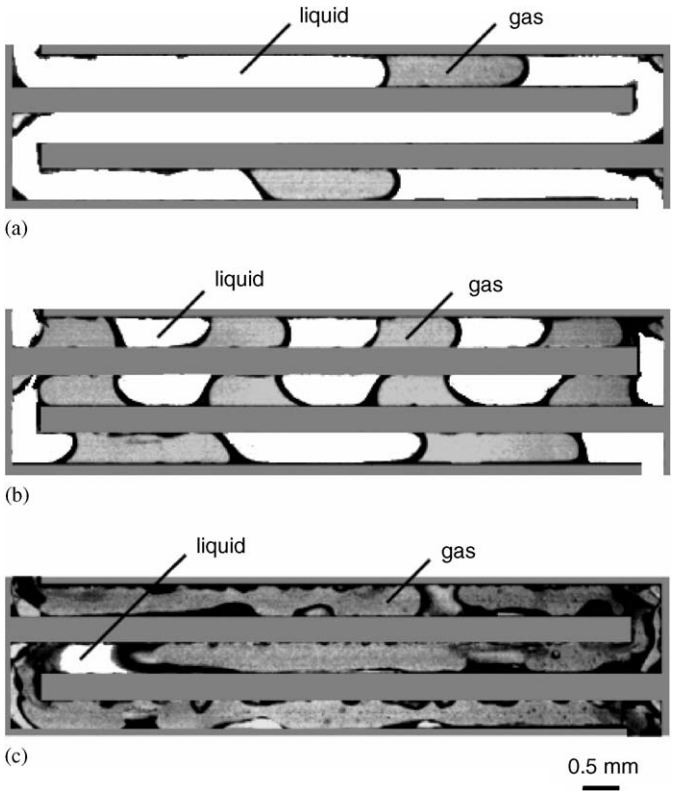

Fig. 5. Pure water/air flow patterns in hydrophobic channels. From low to high void fractions. (a) Isolated asymmetric bubble flow, (b) wavy bubble flow, (c) scattered droplet flow.

(b) For intermediate void fractions, the flow is composed of liquid and gas plugs. Bubbles and droplets are not symmetric in the direction of the flow. Interface instabilities cause asymmetry with respect to the channel axis. A corner can block a bubble until another bubble joins it and forms a bigger one, as shown on the lower channel in Fig. 5(b).

(c) For high void fractions, the flow consists of small liquid droplets adhering to the channel wall, while gas is flowing in the center of the channel. Droplets move randomly. When droplets merge to form a droplet larger than the channel size, the resulting liquid plug is advected by gas flow. This liquid plug collects small liquid droplets in its path.

2.4. Foam flow patterns

When a gas is mixed with a liquid containing one or more surface active agents, a foam is formed. Foams show complex fluid properties depending on their void fraction, bubble size distribution, and chemical composition. Foam may exhibit the behavior of a solid, despite being composed of liquid and gas. Common foam production techniques (Briceño and Joseph, 2003) lead to polydisperse foams. The on-chip mixing section used in our experiments allows the production of monodisperse foams composed of bubbles, of adjustable size. Monodisperse foams confined in channels display ordered structures that

depend on the ratio of the bubble size to the channel width (Drenckhan et al., 2003). Over time, the structure of foam is altered either due to coalescence or coarsening between bubbles of different sizes. For this reason, monodisperse foams show better stability compared to polydisperse foams.

2.4.1. Hydrophilic flows

An aqueous solution of sodium dodecyl sulfate at a concentration of 4.5×10^{-3} mol/l is mixed with air. Foams are classified into two principal categories (Deshpande and Barigou, 2001; Briceño and Joseph, 2003): "dry foams" (Figs. 6(a)–(f)), which have high void fractions; and "wet foams" (Figs. 6(g)–(i)), which have lower void fractions.

Dry foams move as a rigid body. Their bubbles are closely packed and do not move relative to one another. All bubbles move at the same velocity in the microchannel. In this case, the foam flows as a solid core lubricated by water on the walls. For a very high void fraction, the liquid/gas mixer produces long bubbles traveling as a train (Fig. 6(a)). As a function of the ratio of bubble size to channel width, ordered (Figs. 6(a)–(c) and (f)) and disordered (Figs. 6(d) and (e)) flow structures are formed. Among the ordered flows, staircase flows (Fig. 6(b)) and hexagonal-packed flows are observed (Fig. 6(f)). In the case of a disordered structure (Figs. 6(d) and (e)), bubbles form polydisperse polyhedral cells. In this situation, local rearrangements between neighboring bubbles may facilitate coalescence, leading the system to a higher degree of polydispersity. As a general trend, when the bubble size decreases, the number of neighboring bubbles increases, as does the number of facets of each bubble.

As the void fraction decreases, the rheological behavior of the foam changes from a solid to a fluid flow. At intermediate void fractions, the flow is stratified (Figs. 6(g) and (h)). Wet foams are characterized by spherical bubbles that move in relation to one another. For very low void fractions, the flow becomes bubbly, as in the case of pure water (Fig. 6(i)).

2.4.2. Hydrophobic flows

For the case of liquid/gas flows with surfactant in hydrophobic channels, we have identified two principal flow regimes that are a combination of previously described flow patterns: bubbly–droplet flow for high void fractions (Fig. 7(a)); and bubbly–plug flow for low void fractions (Fig. 7(b)):

(a) For the bubbly–droplet flow, moving liquid droplets are stuffed with small gas bubbles. Changing the liquid and gas flow rates induces a change in size and distance between droplets. These droplets are created by collecting multiple droplets where small gas bubbles are trapped.

(b) The bubbly–plug flow is a combination of bubbly and plug flows. The gas plug is moving at the same velocity as the liquid. Consequently, the gas plug pushes small bubbles downstream. As for the bubbly–droplet flow, size and distance between plugs is adjustable by changing the liquid and gas flow rates. For very low void fractions, the flow is bubbly and is frequently perturbed by large plugs pushing all the small bubbles downstream.

Liquid/gas in square microchannels presents a large variety of flow patterns that are strongly correlated to specific channel geometries and properties of the liquid/gas, liquid/solid, and solid/gas interfaces. A wide range of industrial and scientific applications can benefit from precise control of interfacial properties. Flowing the appropriate solvent through the channel can be used to control the solid wall properties. However, when channel dimensions shrink to the characteristic size of the solvent molecules, unexpected two-phase flow occurs.

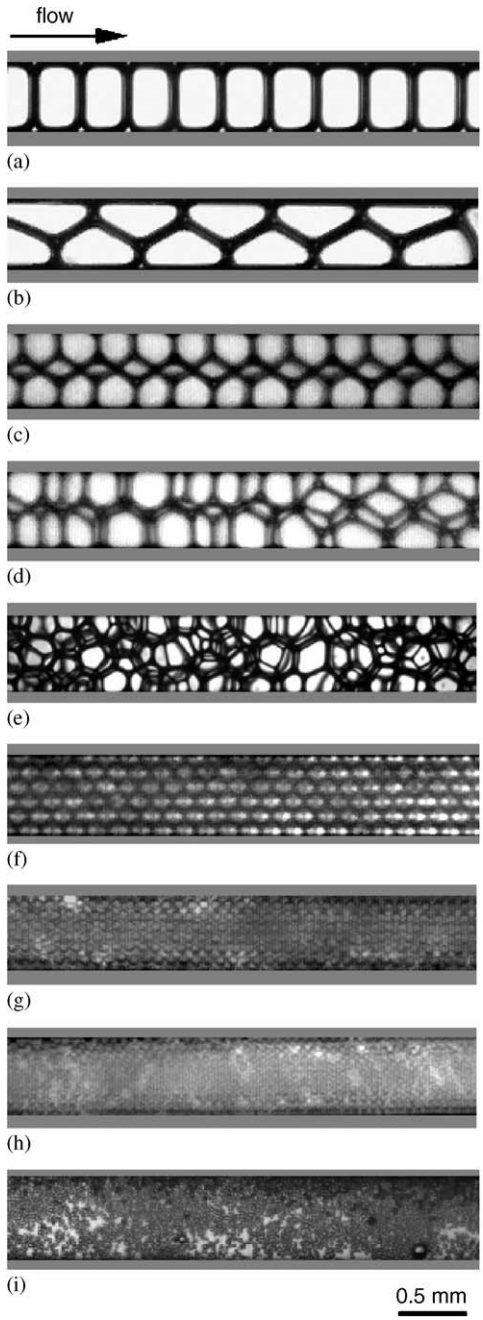

Fig. 6. Water with surfactant/air flow patterns in hydrophilic channels. From high to low void fractions. (a)–(f) Dry foams, (g)–(i) wet foams.

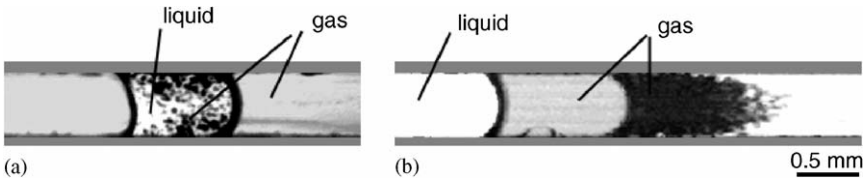

Fig. 7. Water with surfactant/air flow patterns in hydrophobic channels. From high to low void fractions. (a) Bubbly–droplet flow, (b) bubbly–plug flow.

3. Flows of polymer solutions in microgeometries

Surface treatments of fluidic passages are routinely performed inside biochips to optimize several processes. Several liquid/gas flow patterns, which depend on either hydrophilic or hydrophobic surfaces, are reported in previous sections. Another example of the importance of surface modifications is when surfaces treated with polyethylene glycol (Deval, 2002) become inert to some biological species, such as proteins. Proteins would otherwise precipitate, foul the walls of the biochip, and therefore deplete the solution and potentially clog the device. In other situations, surface treatments are performed to obtain the opposite result, namely, capturing specific types of molecules on a substrate. Gau et al. (2001) showed that rRNA molecules, used for the detection of DNA molecules, bind to a gold electrode through a monolayer of Streptavidin molecules grown on a self-assembled monolayer of a biotin-based compound.

3.1. Rheological phenomena observed in microflow configurations

Such treatments are usually performed by flowing a solution through the biochip, usually by injecting the solution into the biochip with a syringe. These solutions contain molecules that will achieve surface modifications at the molecular level after precipitation.

In general, the molecules of both the solvent and the solute are much smaller than the characteristic dimension of the fluidic passages, which are on the order of 100 μm. These solutions can be described as a continuum with a change in the apparent viscosity. However, as the size of the fluidic passages is reduced and becomes comparable to the size of molecules suspended in the solvent, the homogeneous continuum assumption breaks down. In an extreme case, the entropic trapping of DNA molecules forced through much smaller passages has been reported (Han et al., 1999).

It is worth noting that a large difference in size usually exists between the molecules of the liquid (water, ethanol, etc.) and the molecules suspended or dissolved in it (DNA strands, proteins, etc.). When the dimensions of the solute molecules approach the cross-sectional dimensions of the channel, the solvent retains its continuum characteristics. In this scenario, there is a two-phase flow since large individual molecules in a liquid medium are transported individually through small passages.

3.2. Experiments

In our work, we study the rheology of a 1% aqueous solution of 5 M mw PAAm injected through a micron-size capillary, as shown in Fig. 8. The size of the PAAm molecules in their coiled configuration is estimated to be around 0.5 μm.

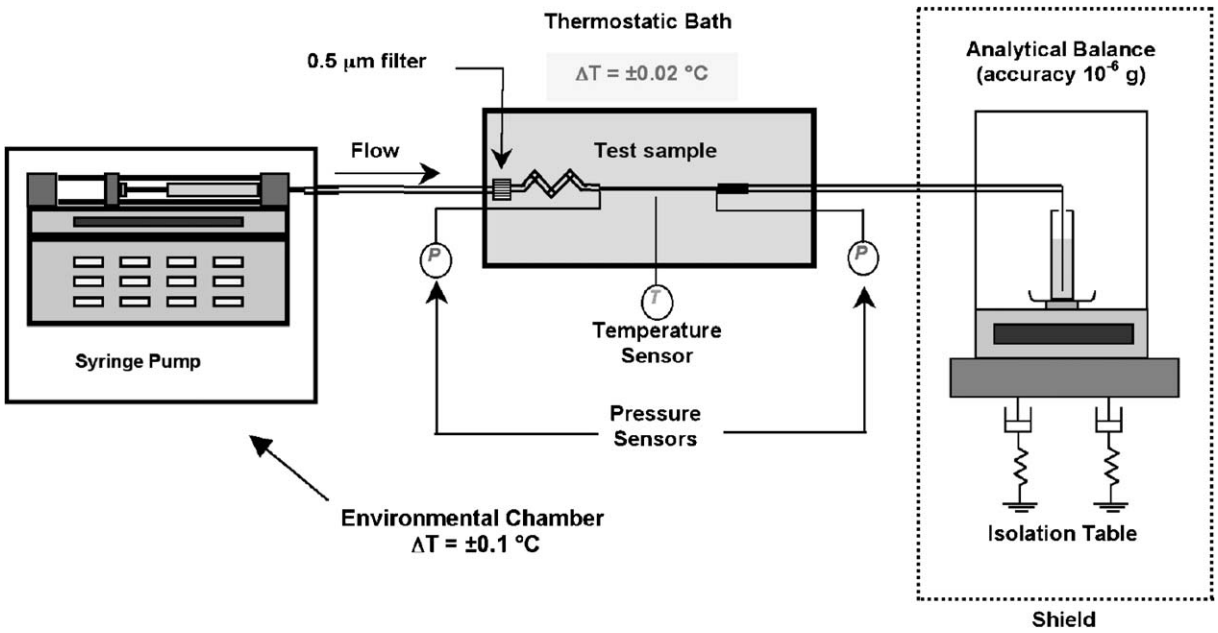

Fig. 8. Experimental setup used to study polymer solutions in microgeometries.

Two different types of extruded silica capillaries are used as test sections. One is 101.5 μm in diameter and 120 mm long, and the other is 10 μm in diameter and 5 mm long. Each capillary is connected to a 10 ml glass syringe placed on a syringe pump. The liquid flowing through the capillary is collected on a vial placed in an analytical balance where the flow rate is determined by time differentiation of the measured weight of collected fluid. The pressure of the liquid is measured upstream and downstream of the capillary. In order to mitigate thermal effects, the syringe and the syringe pump are placed inside an environmental chamber where the temperature is held constant within 0.1 °C. The test section is placed in a thermostatic bath where the temperature is controlled within 0.02 °C.

Starting from the condition where the syringe pump is off and where the pressure drop across the capillary is zero, flow through the test section is initiated by starting the syringe pump at a given constant flow rate Q. Fig. 9 shows the time response recorded for five different values of imposed flow rates, ranging from 0.5 to 0.9 μl/ min, for the smaller capillary, when the size of the polymer is only 20 times smaller than the diameter of the cross-section. The syringe pump is switched off at the point labeled "a" either because a maximum threshold pressure is exceeded, or because the fluctuations in the pressure drop decrease to a certain value. The recorded transients show a peculiar behavior consisting of the presence of two overshoots, one at the end of the initial rise, between 2 and 3 h after the pump is started, and the second between 6 and 9 h after the flow is initiated. Eventually, the pressure proceeds to a steady state with minor oscillations. The fall in pressure drop after the syringe is switched off does not show any peaks or oscillations. The shift of the peaks to smaller time, as the flow rate is increased, suggests a correlation between the characteristic time constant of the polymer suspension, the flow rate and the channel size. For comparison, experiments performed with pure water in 10 μm channels exhibited a monotonous increase of the pressure drop with time after the syringe pump is started (Ulmanella, 2003).

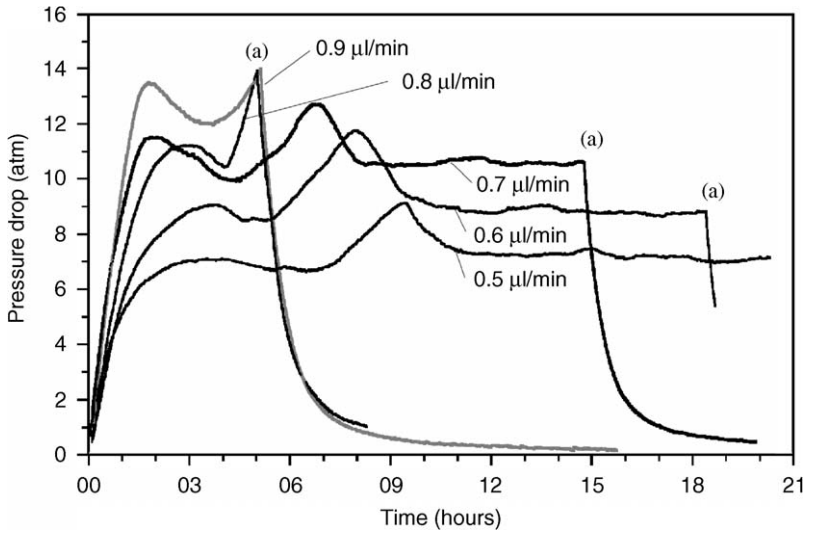

Fig. 9. Recorded time transients for the pressure drop at different values of the imposed flow rate.

The transient of the larger capillary is almost instantaneous, as it takes only a few seconds to reach a true steady state. For the 10 μm capillary, the transient is on the order of 10–12 h, and residual oscillations prohibit a true steady state within the time of our measurements. This time scale may have important implications for performing surface modifications in nanochannels.

For the flow in the small capillary, the rheological behavior of the solution is as unexpected as the time transient. For example, Fig. 10 shows the measured pressure drop, the measured mass flow rate actually flowing through the capillary, and the calculated viscosity of the solution, as a function of time, for $Q = 0.9\,\mu\text{l}/\,\text{min}$ and similar test conditions as above. Plots are also obtained for other values of flow rates.

Several anomalies can be noticed in the plot. First, between "a" and "b", the measured mass flow rate remains constant while the pressure drop continues to increase, leading to a dramatic increase in viscosity. Second, between "c" and "e", the pressure drop decreases while the mass flow rate increases. At "d", the viscosity drops almost to the same value as that at $t = 0$. Also, the actual flow rate occurs to be up to 10% larger than the flow rate dispensed by the syringe pump. Third, after the syringe pump is stopped at "e", there is a discontinuity in the mass flow rate during the pressure decay transient at "g". At this moment, the sudden increase in the mass flow rate causes a drop in the viscosity, which reaches approximately the same value as that at $t = 0$.

As illustrated in Fig. 11, these anomalies reflect an unexplained hysteretic behavior and a non-linear relationship between pressure drop and flow rate between points "a" and "g".

The dramatic impact of the flow length scale on the PAAm solution is clearly visible in Fig. 12. The experimental master curve (apparent viscosity vs. shear rate) for the flow in the 10 μm capillary is compared to the classical behavior (dotted line) of the same type of solution (Kulicke et al., 1982) at $T = 25\,^{\circ}\text{C}$. In general, when the cross-sectional dimension of the flow is much larger than the polymer molecules suspended in the solution, the value of the viscosity coefficient of the diluted polymer solution is constant below a critical shear rate. Above the critical shear rate, the solution shows a "shear-thinning"

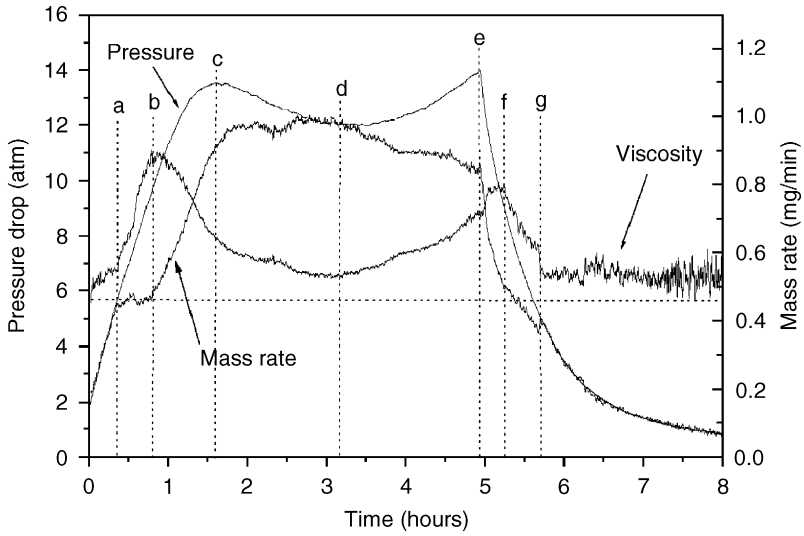

Fig. 10. Time transients of pressure drop, mass flow rate, and calculated viscosity at $Q = 0.9\,\mu\text{l}/\,\text{min}$. The syringe pump is started at $t = 0$ and stopped at "e".

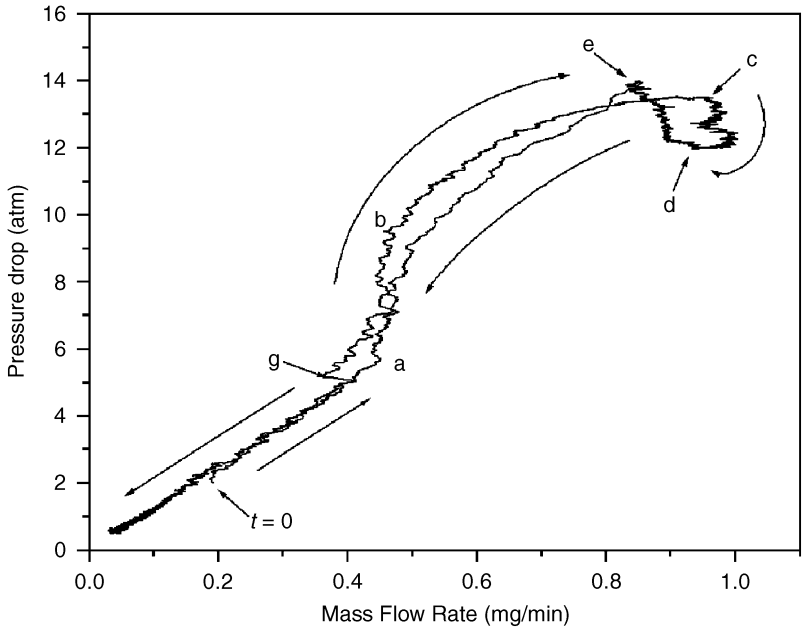

Fig. 11. Pressure drop versus mass flow rate.

behavior, i.e. a decrease in viscosity with the shear rate, due to the unfolding of the coiled polymer molecules by internal shear stresses. For a PAAm solution like the one used in the present experiment, the shear-thinning starts at $\gamma \approx 1\,\text{s}^{-1}$. In our experiment, the viscosity is several times larger than the

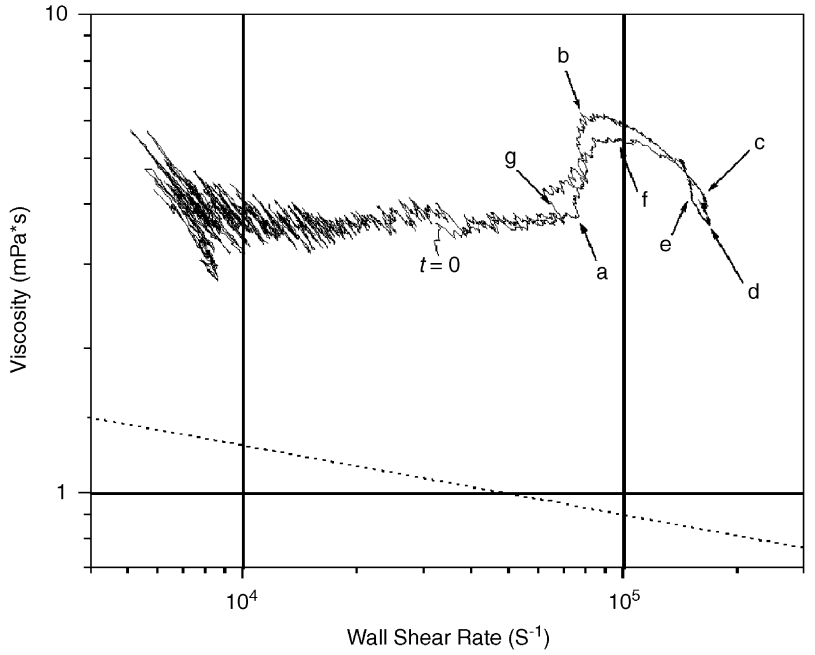

Fig. 12. Master curve for the polymer solution obtained from the transient response. The dotted line represents the expected behavior.

expected value, and does not show the traditional shea-thinning behavior. Instead, the viscosity exhibits a quick increase between “a” and “b”, followed by a drop between “b” and “d”.

4. Conclusion

This paper presents two types of multiphase flows in microchannel geometries. We investigated the shape of static elongated bubbles in square channels for different contact angles. When liquid and gas are flowing in microchannels, dynamic contact angles play an important role in the selection of the flow regime. We described liquid/gas flow patterns obtained with an on-chip liquid/gas mixer in square microchannels with surface modifications (hydrophobic/hydrophilic). Pure water and air, as well as water with surfactant and air flow patterns were investigated and showed a rich variety of regimes. This study reveals the importance of surface treatments for multiphase flows at the microscale. In addition, we investigated large macromolecules flowing through micron-sized channels. Under such conditions, the transient behavior of a PAAm solution displays anomalous features. The unexpected behavior suggests an unsteady response of the macromolecules. A parametric investigation of the dependence of the time response on the channel size and molecular weight of the polymer may help us to understand these phenomena. The unusually long transient times associated with impulsively started flows in microchannels suggest a complex interplay between the shear-thinning viscoelastic properties of the fluid and the channel size. A systematic study of these effects using micro- and nanofluidic devices would provide useful insights on the rheology of polymer suspensions and more generally on soft-condensed mater. In conclusion, our

results demonstrate that the reduction in size of the channels dramatically enhances the effects of the walls on two-phase flows. In particular, the bulk two-phase flow becomes largely dependent upon the walls' interfacial properties. It is likely that understanding multiphase flow behaviors at the microscale would not only provide significant scientific insight but also offer new functionalities for practical uses in domains as diverse as micropower generation, chemical engineering, and bio-detection in microfluidics.

Acknowledgments

This work was supported by DARPA/MTO, "Micro Power Generation" program, the NSF NIRT program and the CMISE Institute (a NASA URETI).

References

Briceño, M.I., Joseph, D.D., 2003. Self-lubricated transport of aqueous foams in horizontal conduits. Int. J. Multiphase Flow 29, 1817–1831.

Concus, P., Finn, R., 1974. On capillary free surfaces in absence of gravity. Acta Math. 132, 177.

Cubaud, T., Fermigier, M., 2004. Advancing contact lines on chemically heterogeneous surfaces. J. Colloid Interface Sci. 269, 171–177.

Cubaud, T., Ho, C.-M., 2004. Transport of bubbles in square microchannels. Phys. Fluids 16 (12), 4575–4585.

Cubaud, T., Tatineni, M., Zhong, X., Ho, C.-M., 2005. Bubble dispenser in microfluidic devices. Phys. Rev. E 72, 037302.

Deshpande, N.S., Barigou, M., 2001. The flow of gas–liquid foams through pipe fittings. Int. J. Heat Fluid Flow 22, 94–101.

Deval, J., 2002. Electrokinetic sub-micron particle manipulation for micromixing in bioreactors. Ph.D. Thesis, University of California, Los Angeles.

Deval, J., Ulmali, T.A., Lan, E.H., Dunn, B., Ho, C.-M., 2004. Reconfigurable hydrophilic/hydrophobic surfaces in microelectromechanical systems (MEMS). J. Micromech. Microeng. 14, 91–95.

Drenckhan, W., Elias, F., Hutzler, S., Weaire, D., Janiaud, E., Bacri, J.-C., 2003. Bubble size control and measurement in the generation of ferrofluid foams. J. Appl. Phys. 93 (12), 10078–10083.

Gau, J.J., Lan, E.H., Dunn, B., Ho, C.-M., Woo, J.C.S., 2001. A MEMS based amperometric detector for E-Coli bacteria using self-assembled monolayers. Biosensors Bioelectron. 16 (9–12), 745–755.

Han, J., Turner, S.W., Craighead, H.G., 1999. Entropic trapping and escape of long DNA molecules at submicron size constriction. Phys. Rev. Lett. 83 (8), 1688–1691.

Kolb, W.B., Cerro, R.L., 1993. The motion of long bubbles in tubes of square cross section. Phys. Fluid A 5 (7), 1549.

Kulicke, W.-M., Kniewske, R., Klein, J., 1982. Preparation, characterization, solution properties and rheological behaviour of polyacrylamide. Prog. Polym. Sci. 8, 373–468.

Link, D.R., Anna, S.L., Weitz, D.A., Stone, H.A., 2004. Geometrically mediated breakup of drops in microfluidic devices. Phys. Rev. Lett. 92 (5), 54503.

Thorsen, T., Roberts, R.W., Arnold, F.H., Quake, S.R., 2001. Dynamic pattern formation in a vesicle-generating microfluidic device. Phys. Rev. Lett. 86 (18), 4163.

Ulmanella, U., 2003. Molecular effects on the boundary condition in micro and nano fluidic channels. Ph.D. Thesis, University of California, Los Angeles.

Yen, T.J., Zhang, X., Lu, G.Q., Wang, Y., 2003. A micro methanol fuel cell operating at near room temperature. Appl. Phys. Lett. 83 (19), 4056.